*Exp. Theo. NANOTECHNOLOGY* 7 (2023) 17 - 40 https://doi.org/10.56053/7.1.17

# Investigation of structural and optical properties of In-doped AlSb nanostructures

*S. Radiman*[1,*], *M. Rusop*[2]

[1]Department of Physics, Faculty of Science, National University of Malaysia, Selangor, Malaysia
[2]Department of Physics, School of Applied Science, University Technology Mara, Selangor, Malaysia
*) Email: srphy@ukm.edu.my

*Received* 13/8/2022, *Accepted*, 3/12//2022, *Published* 15/1/2023

---

The first-principles calculations are made to study the structural electronic and optical properties of indium-doped aluminum antimonide. The most appropriate method of density functional theory (DFT) naming Full Potential Linearized Augmented Plane Wave (FP-LAPW) is used. The structural properties like Lattice constant (a), pressure derivative, and bulk modulus (B) were examined by Local density approximation (LDA) along with generalized gradient approximation (GGA). Generalized gradient approximation along with TB-mBJ is used to determine electronic parameters like band structure along and density of states. According to the computed results the binary compound AlSb is optically inactive and exhibits an indirect (Γ-L) band gap. By increasing the concentration of indium with different percentages, the indirect band gap shifted to the direct (Γ – Γ) band gap which shows the material is optically active. The optical properties of the material including dielectric (Real and imaginary parts) constant, reflectivity, refractive index, energy loss, absorption coefficient, and optical conductivity have changed significantly. Electronic and optical properties are modified by (TB-mBJ) approach. The results obtained are examined with experimental data and utilized as a starting point to propose that the material is the superlative choice for the manufacturing of p-n junctions, photo-detectors, laser, photo-diodes, transistors and solar spectrum absorptions in the visible, infrared and ultraviolet energy ranges.

---

**Keywords:** DFT; Structural; Electronic.

## 1. INTRODUCTION

Semiconductor alloys presented an important role in manipulative the material properties by selecting suitable alloy constituents and considered as essential material for the development of new technologies, including photo detectors[1], solar cell devices, and LEDs (light-emitting diodes) [1]. Due to their potential for a wide range of applications semiconductor materials have attracted significant research attention during the past few decades. II-VI, IV-IV, and III-V are among the many types of semiconductors used very commonly. Solar cells, LEDs, photodetectors, laser diodes, LEDs, microelectronic, spintronic, photonic, and optoelectronic devices are a few examples of modern technological devices. These applications are very appealing and motivate us to study the major properties of semiconductors. [2-3]. III-V semiconductors have generated significant interest among diverse contenders due to their numerous technological advancements in a variety of applications, such as high-speed electronics and optoelectronic devices[4]. These semiconductors show crystalline behavior in both the wurtzite phase and zinc blend (ZB). However, the majority of the semiconductors of group III and group V consist of ZB (Zinc Blend) structure[4]. The group III-V family shows a band gap of 2.5 eV or below. Due to these special features such as wide band gap, low effective electronic mass, high thermal conductivity, high electric field, high electronic mobility[5], and strong resistance to radiation, these materials are considered to have great interest in the semiconductor industry[2-3]. Zinc blend crystalline aluminum antimonide (AlSb) belongs to indirect band gap semiconductor material with a 1.669 indirect band gap value [8] and a lattice parameter of 6.135 (Å) [9]. This small band gap suppresses radiative recombination and gives the electron-hole pair more time for detection. Also due to their high electronic mobility, AlSb is widely used to make other electronic devices for high-temperature applications such as p-n junctions, diodes, laser, and solar spectrum absorption [10] the potential absorber, and is commonly suitable for solar energy devices [11].

Recently, Dhakal et al. prepared fine AlSb by supporting aluminum and antimony together and showed that the binary alloy AlSb is a promising photovoltaic material[9]. Tang et al. investigated the structural, electronic (represents the band gap), and optical properties of binary alloy AlSb thin film deposited by laser deposition. Relevant theoretical work has been done recently on mixed ternary crystals. In addition to the experimental field, the theoretical field is used to get an improved understanding of the physical properties of materials. Different authors studied the ternary (AlGaSb, GaBP, etc.) alloys formed by replacing the Gallium (Ga) atom with other group IIIA atoms at varying concentrations in the GaP crystal using density functional theory [12]. Recently, Zhang et al. studied the structural, mechanical, and electronic properties of ternary alloys $Ga_{1-x}B_xP$ ($x = 0.0, 0.25,\ 0.5,\ 0.75, and\ 1$) using the plane wave pseudopotential method [13].

Othman deliberated the structural, optical, and electronic properties of $In_xGa_{1-x}As$ alloys using the ab-initio/first principle plane-wave pseudo potential method at x = 0 and 0.5 only[12]. Shen premeditated the optical properties, electronic properties, and structural properties of $In_xGa_{1-x}P$ with a concentration range from 6.25% to 25% using CA-PZ form of local density approximation (LDA)[8]. An alloy in a semiconductor can be defined as a compact solution of two or more semiconductors by accretion of different percentages [14]. The addition of doping atoms at varying percentages makes pure semiconductors more significant and attractive for their optoelectronic applications. The objective of this research is to examine the structural , electronic and optical properties of $Al_{1-x}In_xSb$ (X =0, 0.25, 0.50, 0.75) semiconductor alloy in the mixed zinc phase and mark it suitable for optoelectronic devices [15].

## 2. COMPUTATIONAL METHOD

The physical Properties of In-doped AlInSb is carried using Density functional theory with the assistance of WIEN2k code package [16]. In density functional theory full potential linearized augmented plane wave (FP-LAPW) method implemented in WIEN2K code[17] is used. Pedrew-burke and Ernzerh generalized gradient (GGA-PBE) approach is employed by taking into account of the local density approximation (LDA) to calculate structural, optical, and electronic properties[7]. However electronic and optical properties are modified by Tran and Blaha Becke-Johnson's approach [18]. A super cell of 1x1x1 with RMT value 4 has been generated for eight atoms of AlSb. The space group for the Zinc blend structure of AlSb and alloys is 216_F43-m[13] and the separation energy of core/valance shells is -0.6. No spin-polarized calculations are performed to get optimization value in the volume energy curve. In the muffin-tin spheres, the basis functions, electron densities, and potentials were enlarged along with the spherical harmonic functions with a cut-off of lmax = 10 charge density was given by Fourier as $G_{max}$ =12. This approach selects Rmt Kmax = 7 as the parameter that determines the size of the matrix[19]. The radius of the muffin-tin sphere varies with the alloys as it is taken 3 for binary alloys and 4 for ternary alloy [20]. To calculate electronic properties a Brillion zone of 1000 k-points is to ensure self-consistency[21]. We used $10^{-7}$ Ry for the convergence of the total energy criterion[22]. Total energy calculations are made using the full potential linearized augmented plane wave (FP-LAPW) method. In this method, the unit cell is divided into non-overlapping muffin regions and interstitial sites[8-20]. The wave function in the muffin-tin region is probably atomic-like whereas there is a plane-wave basis in the interstitial region.[24]. The application of LDA and GGA to solids can also result in findings that are significantly out of sync with experiment, such as severely underestimating or even missing the band gap of semiconductors and insulators. More generally, the derivative discontinuity of the exchange-correlation potential xc causes the band gap derived from the eigenvalue spectrum to deviate from the actual band gap (the ionization potential I minus the electron affinity A), which is the potential that is the same for all orbitals. Other functional or techniques can be used to calculate band gaps that are better[25].The Kohn-Sham equation is used for energy and correlation potential change[8]. Semi-local approaches produce results that are sufficiently precise to interpret experimental data also they are computationally inexpensive[25]. The Kohn-Sham band gap does not match the experimental band gap when computing the electronic properties of $Al_{1-x}In_xSb$(x= 0,0.25,0.5.0.75) using GGA-PBE because the ionization potential is subtracted from the electron affinity [26]. To resolve this difficulty effective potential of Tran–Blaha-modified Becke–Johnson (TB–mBJ) built-in Wien2k is used [25-26]. Modified Becke-Johnson potential can be used to enhance the band gaps obtained by traditional and standard DFT-based approaches[20]. Band gaps of semiconductors, semi-metals, transition metal oxides, broadband insulators, and doped semiconductors can be precisely determined using this method[28] which is represented as;

$$v_{x,\sigma}^{TB-mBJ}(r) = \left(1.023\sqrt{\frac{1}{\pi}\int\frac{|\nabla\rho_\sigma(r')|}{\rho_{\sigma(r')}}dr'} - 0.012\right) \text{ x } \left\{\frac{2\sqrt[3]{\pi\rho_\sigma(r)}\,e^{\frac{x_\sigma(r)}{3}}}{x_\sigma(r)} \times \left[\left(1+\frac{1}{2}x_\sigma(r)\right)e^{-x_\sigma(r)} - 1\right] + \frac{3}{\pi}\sqrt{\frac{5}{12}}\left(\frac{\sum_{i=1}^{N}\nabla\psi_{i,\sigma}^{*}\nabla\Psi_{i,\sigma}}{\sum_{i=1}^{N_\sigma}|\psi_{i,\sigma}|^2}\right)\right\} - \frac{2}{\pi}\sqrt{\frac{5}{12}}\left(\frac{\sum_{i=1}^{N}\nabla\psi_{i,\sigma}^{*}\nabla\psi_{i,\sigma}}{\sum_{i=1}^{N}|\psi_{i,\sigma}|^2}\right)^{\frac{1}{2}}$$

$$= \text{ c x } \left(v_{x,\sigma}^{BJ}(r) + \frac{1}{\pi}\sqrt{\frac{10t_\sigma(r)}{3\rho_{\sigma(r)}}}\right) - \frac{1}{\pi}\sqrt{\frac{10t_\sigma(r)}{3\rho_\sigma(r)}} \qquad \textbf{(1)}$$

**Ω** denotes unit cell volume and $\rho_\sigma(r)$ referred charge density of electron $\rho_\sigma(r) = \sum_{i=1}^{N_\sigma}|\psi_{i,\sigma}|^2$, $x_\sigma$ associated with topology of charge density and can be calculated from $\rho_\sigma(r)$, $\nabla\rho_\sigma$, and $\nabla^2\rho_\sigma$ is a gradient with laplacian of electron,s charge density also $t_\sigma(r) = \frac{1}{2}\sum_{i=1}^{N}\nabla\psi_{i,\sigma}^{*}\nabla\Psi_{i,\sigma}$ is the kinetic energy density of electron. Where $v_{x,\sigma}^{TB-mBJ}(r)$ denotes exchange potential concerning exchange potential $v_{x,\sigma}^{TB}(r)$, if constant c=1 than $v_{x,\sigma}^{TB-mBJ}(r) = v_{x,\sigma}^{TB}(r)$. The above relation satisfies that local density approximation (LDA) and generalized approximations (GGA) are employed mainly to create exchange-correlation energy. Exchange energy functional $E_x$ is used to obtain (TB–mBJ) exchange potential $V_{x,\sigma}^{TB-mBJ}(r) \neq \frac{\delta E_x}{\delta\rho_\sigma}$. Equation 1 states that the c-factor is based linearly on the average value's square root.$\frac{|\nabla\rho_\sigma|}{\rho_\sigma}$ .The c-factor correction is self-consistently converged in the TB-mBJ calculation, and the measured value is so minimal that the band gap value achieved is also modest in comparison to the experimental band gap intended for semiconductors. For all compounds, the c-factor affects electron density and determines the band gap value.

## 3. RESULTS AND DISCUSSION

### *3.1 Structural properties*

The structural optimization of binary compound (AlSb) and ternary alloys ($Al_{1-x}In_xSb$) are calculated by manipulating the total energies at several volumes about equilibrium cell volume $V_0$. Our deliberated values of lattice parameters are 6.158A˚ 6.265A˚, 6.360 A˚ and 6.435 A˚ for AlSb, $Al_{0.75}In_{0.25}Sb$, $Al_{0.5}In_{0.5}Sb$, and $Al_{0.25}In_{0.75}Sb$ respectively.

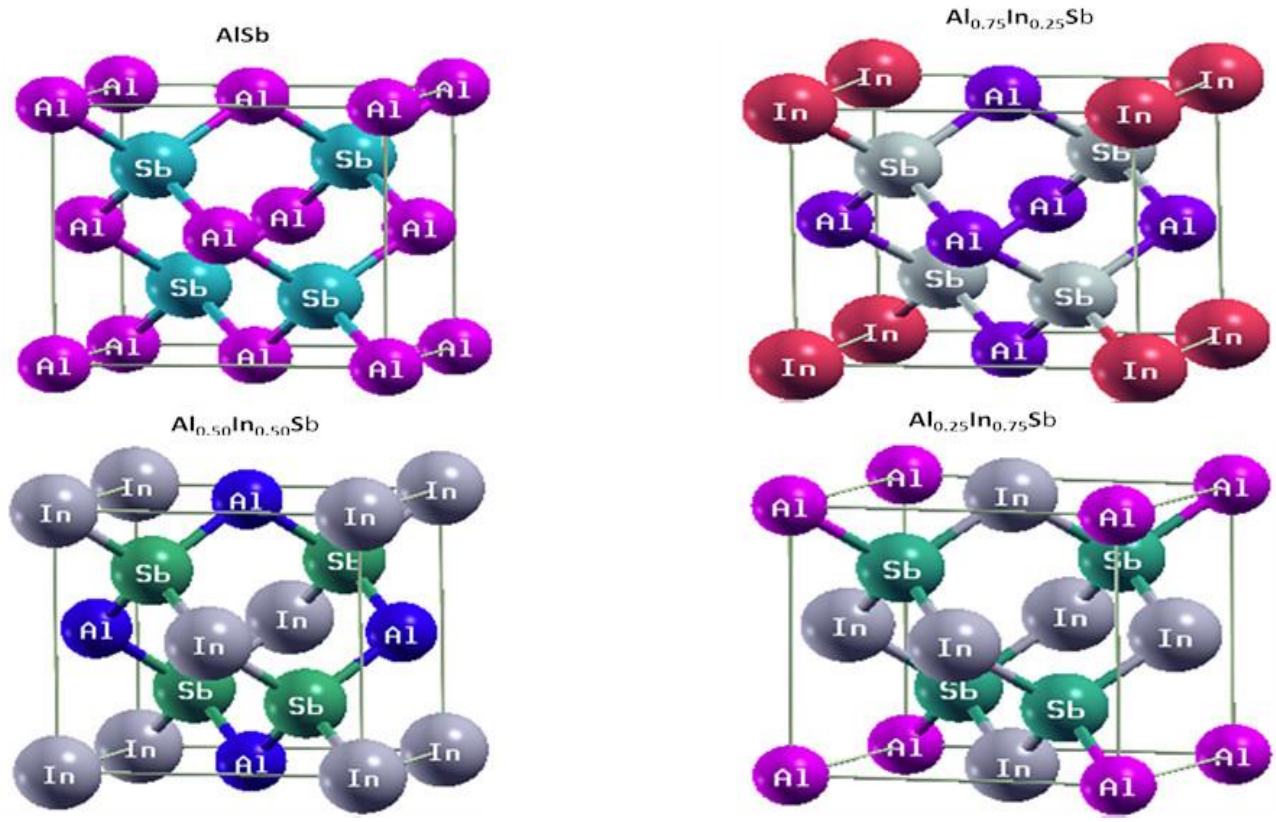


**Figure 1**: Crystal structure of AlSb, $Al_{0.75}In_{0.25}Sb$, $Al_{0.5}In_{0.5}Sb$, and $Al_{0.25}In_{0.75}$ Sb super cell.

The Muranghan equation of state is used to derive structural properties such as the ground state energy ($E_o$), lattice constant (a), ground state volume ($V_0$), pressure derivative (B'), and bulk modules (B) by minimizing the total crystal energies.[29].

$$E(V) = E_O + \frac{B_O V}{\acute{B}_O}\left[\frac{(V_O/V)^{\acute{B}_O}}{B_O\acute{} - 1} + 1\right] - \frac{B_O V}{B_O\acute{} - 1}$$

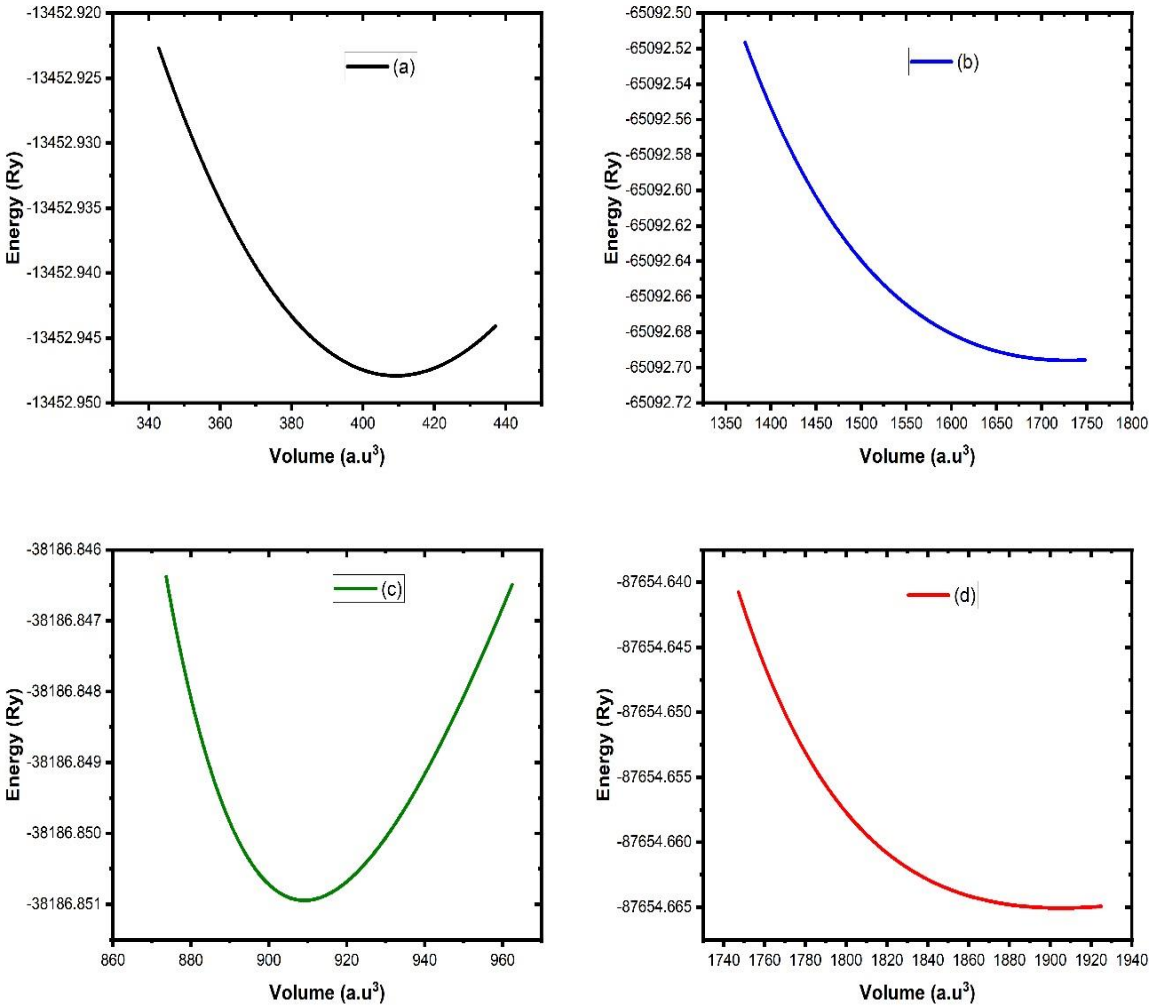


**Figure 2** Optimization of energy as a function of unit cell volume for (a) AlSb (b)$Al_{0.75}In_{0.25}Sb$ (c) $Al_{0.5}In_{0.5}Sb$ and(d) $Al_{0.25}In_{0.75}Sb$.

The structure optimization curve shows that increasing the volume reduces the energy up to the ground state value. As the volume continues to increase, the energy of the unit cell increases and the system moves towards volatility as shown in Fig 2. A proportional analysis of ground state factors such as the bulk modulus, lattice constant, and pressure derivative for AlSb and ternary alloy $Al_{1-x}In_xSb$ an (x =0, 0.25, 0.50, 0.75) with other theoretical (Literature) and experimental (Literature) studies are shown in Table 1.

**Table 1** Comparison of calculated Bulk modulus ($B_o$), lattice parameter (a), and pressure derivative ($B'$) of AlSb, $Al_{0.75}In0._{25}Sb$, $Al_{0.5}In_{0.5}Sb$, and $Al_{0.25}In_{0.75}Sb$ with other work

| Alloy | | Lattice Constant a (Å) | Bulk Modulus $B_o$ (Gpa) Pressure derivative ($B'$) |
|---|---|---|---|
| AlSb | Present work | 6.236 | 58.8 4.59 |
| | Experimental Work | 6.2365[30] | 55.1[31] 4.55[31] |
| | Other Theoretical work | 6.230[32] | 49[32] 4.01 [32] |
| | | 6.09[33] | 58.1[34] 3.93[34] |
| | | 6.1669[35] | 54.4116[35] 4.1091[35] |
| | | 6.1184[35] | 54.4378[35] 4.2531[35] |
| $Al_{0.75}In_{0.25}Sb$ | Present work | 6.352 | 31.155 10.58 |
| $Al_{0.5}In_{0.5}Sb$ | Present work | 6.460 | 28.83 6.41 |
| $Al_{0.25}In_{0.75}Sb$ | Present work | 6.6619 | 20.04 6.399 |

The lattice constant of AlSb is increased by increasing Indium atoms concentration for $Al_{0.75}In_{0.25}Sb$, $Al_{0.50}In_{0.50}Sb$, and $Al_{0.25}In_{0.75}Sb$ as shown in Fig. 3.

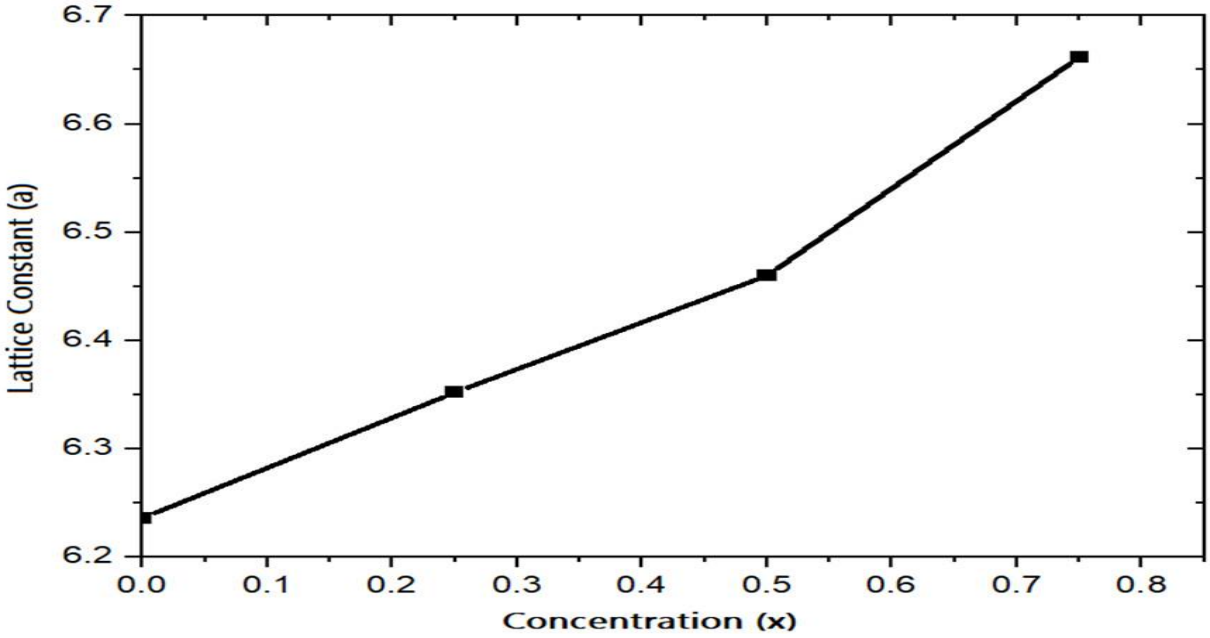


**Figure 3**: Concentration dependence of lattice constant Of $Al_{1-x}In_xSb$**.**

The bulk modulus is an indicator of a material's stiffness. Stronger materials have a higher modulus of compressibility [36]. The binary combination AlSb has a very remarkable bulk modulus of 58.7 because Al and Sb have a strong covalent connection that becomes stronger with increasing indium concentration.

*3.2 Electronic properties*

We analyze the electronic characteristics such as band structure and DOS (density of states) of $Al_{1-x}In_xSb$ (x = 0, 0.25, 0.50, and 0.75) using the Perdew-Burke-Ernzerh (PBE) version of GGA (Generalized Gradient Approximation) and TB-mBJ (Tran-Blaha-modified Becke-Johnson) approach.

*3.2.1 Band structure*

The band-gap energy is an essential device parameter because of sturdily connected with the operating wavelength of optoelectronic devices [21].Tran–Blaha-modified Becke–Johnson (TB–mBJ) approach modifies the band gap of semiconductor materials after the prosperous use of GGA. In AlSb binary alloy the valence band maxima are at a point of Γ symmetry and the conduction band minima Camelback at a point of L symmetry(Γ-L) shows that AlSb has an indirect band gap and the material is optically dormant [9-28]. However, by introducing Indium concentrations as in ternary alloy $Al_{1-x}In_xSb$ (x = 0, 0.25, 0.50, or 0.75), the minima of the conduction band (CB) and the maxima of the valence band (VB) shifted at same symmetry point (Γ-Γ). The transformation occurs from an indirect band gap to a direct band gap and the material becomes optically active [36]. According to Figure 4, the indirect band gap of pure AlSb combination is $1.686\ eV$ but $_{0.75}$ $In_{0.25}Sb$, $Al_{0.50}In_{0.50}Sb$, and $Al_{0.25}In_{0.75}Sb$ have direct electronic band gaps of 1.125 eV$1.08\ eV$ $and$ $.02\ eV$ , resptively.

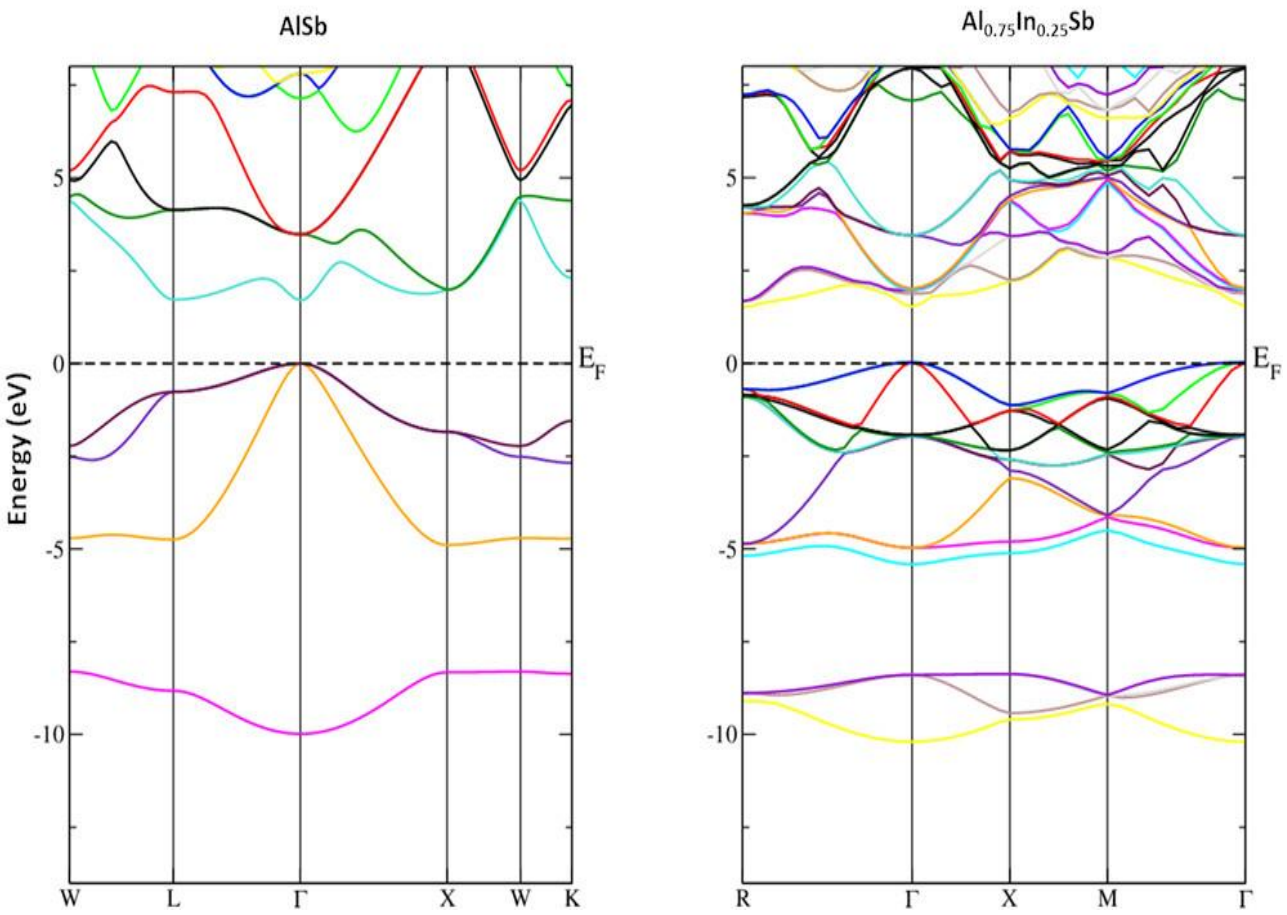


**Figure 4** Electronic Band structure AlSb and $Al_{0.75}In0._{25}S$.

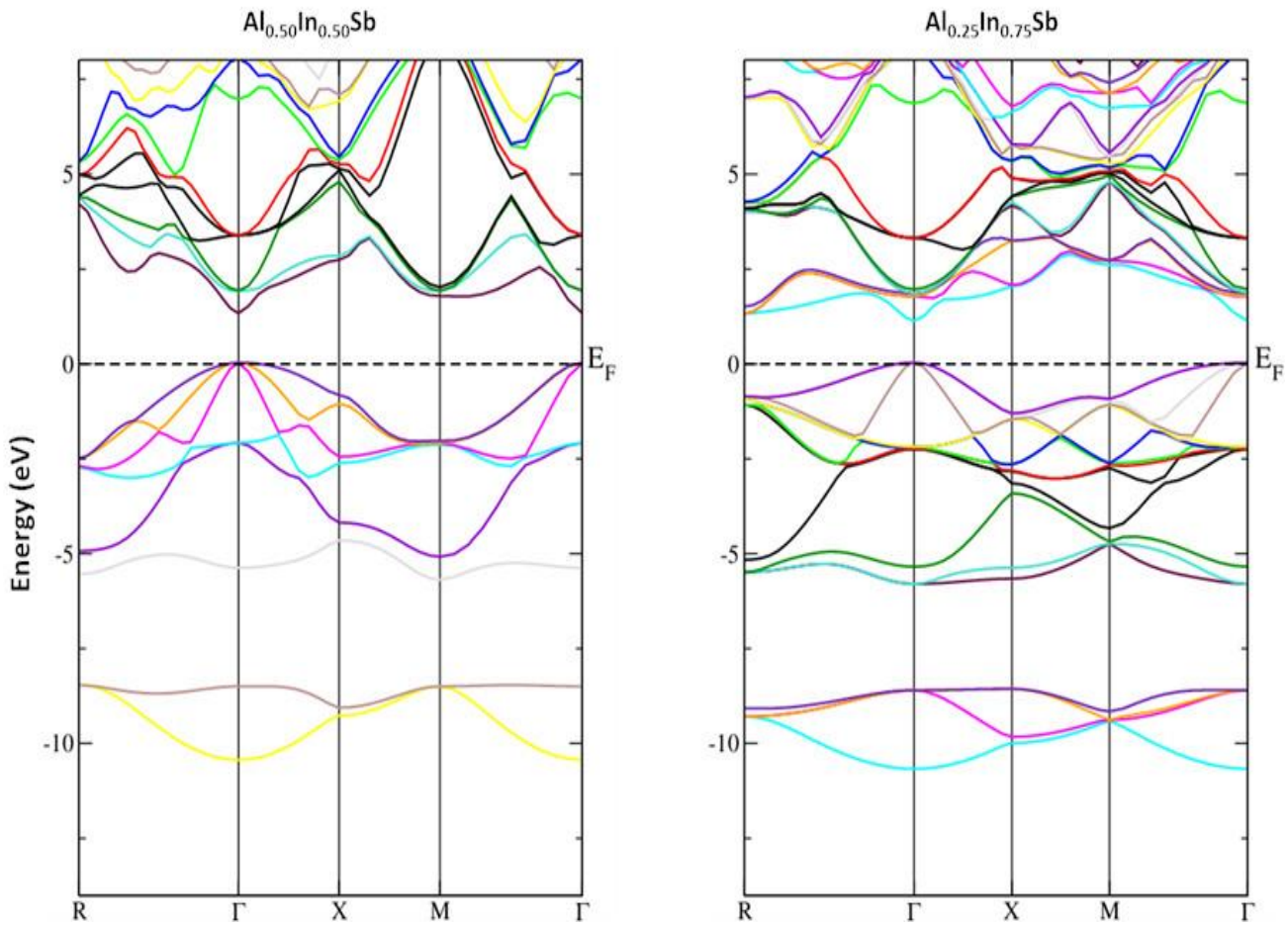


**Figure 5** Electronic Band structure for $Al_{0.5}\,In_{0.5}\,Sb$ and $Al_{0.25}\,In_{0.75}\,Sb$.

Table 2 demonstrates a comparison between the calculated band gap with previous theoretical and experimental studies.

**Table 2** Comparison of Band-gap for AlSb, $Al_{0.75}In0._{25}Sb$, $Al_{0.5}In_{0.5}Sb$ and ,$Al_{0.25}In_{0.75}Sb$ with other work

| Alloy | | Band Gap (eV) |
|---|---|---|
| AlSb | Present work | 1.686 |
| | Experimental Work | 1.6[35] |
| | Other computational work | 1.47[37] |
| | Other computational l work | 1.835[32] |
| | Other computational l work | 1.746[38] |
| | Other computational work | 1.343[37] |
| | Other computational l work | 1.805[39] |
| $Al_{0.75}In_{0.25}Sb$ | Present work | 1.125 |
| $Al_{0.5}In_{0.5}Sb$ | Present work | 1.08 |
| $Al_{0.25}In_{0.75}Sb$ | Present work | 1.02 |

The band gap decreases as the Indium concentration in AlSb increases and the behavior of the material changes from semiconductor to metal. Materials having band gap lower than 3.1 eV shows extremely excellent performance in the visible range of the electromagnetic spectrum. [6]. The relationship between the calculated band gap and the concentration is shown in Figure 6.

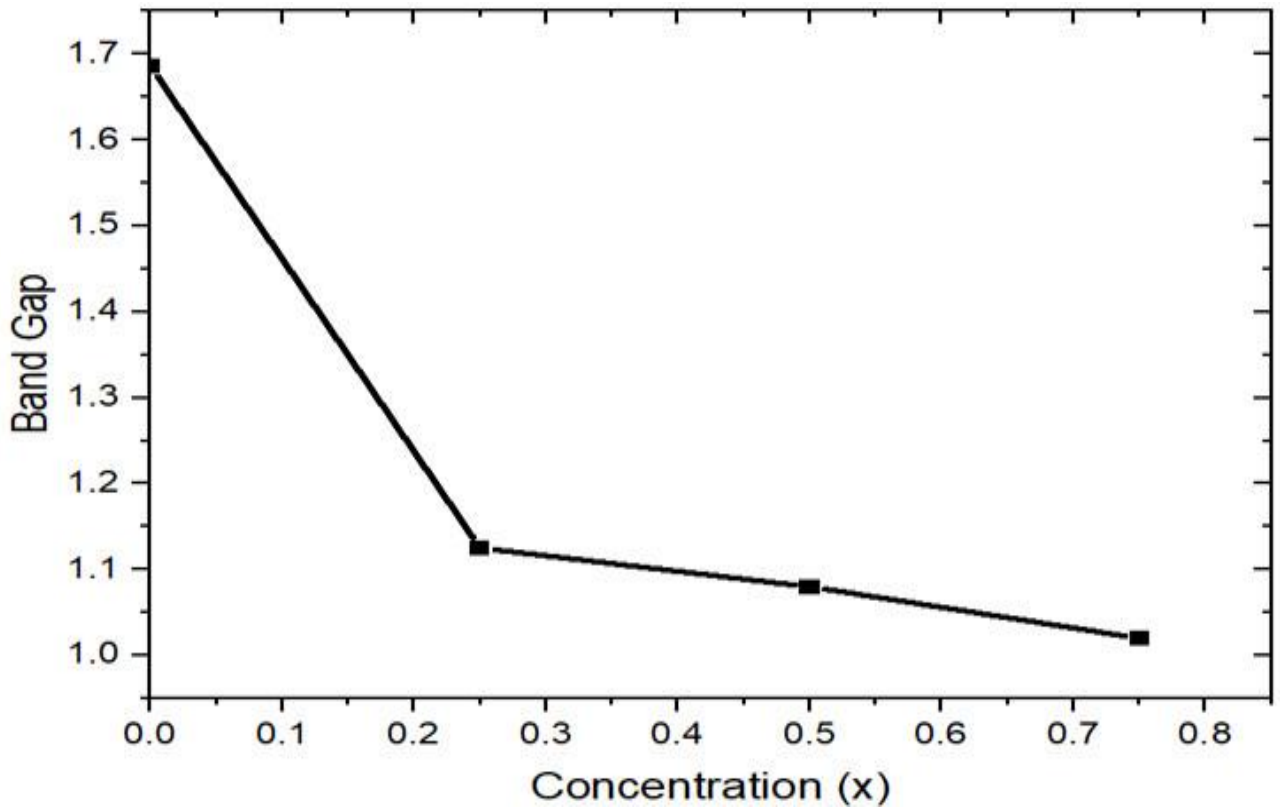


**Figure 6** Variation of band-gap with concentration for $Al_{1-x}In_xSb$**.**

*3.2.2. Density of states*

The contribution of the different valence bands and conduction band electronic states influences the electronic properties [40]. The participation of partial electronic states is used to calculate the total density of the states. The band gap in AlSb and the ternary alloy $Al_{1-x}In_xSb$ in concentration (x = 0.25, 0.50, 0.75) may also be roughly estimated using the density of states [41]. Figure 7 shows the total and the partial density of states for AlSb and $Al_{0.75}In_{0.25}Sb$ calculated using the TB-mBJ approach.

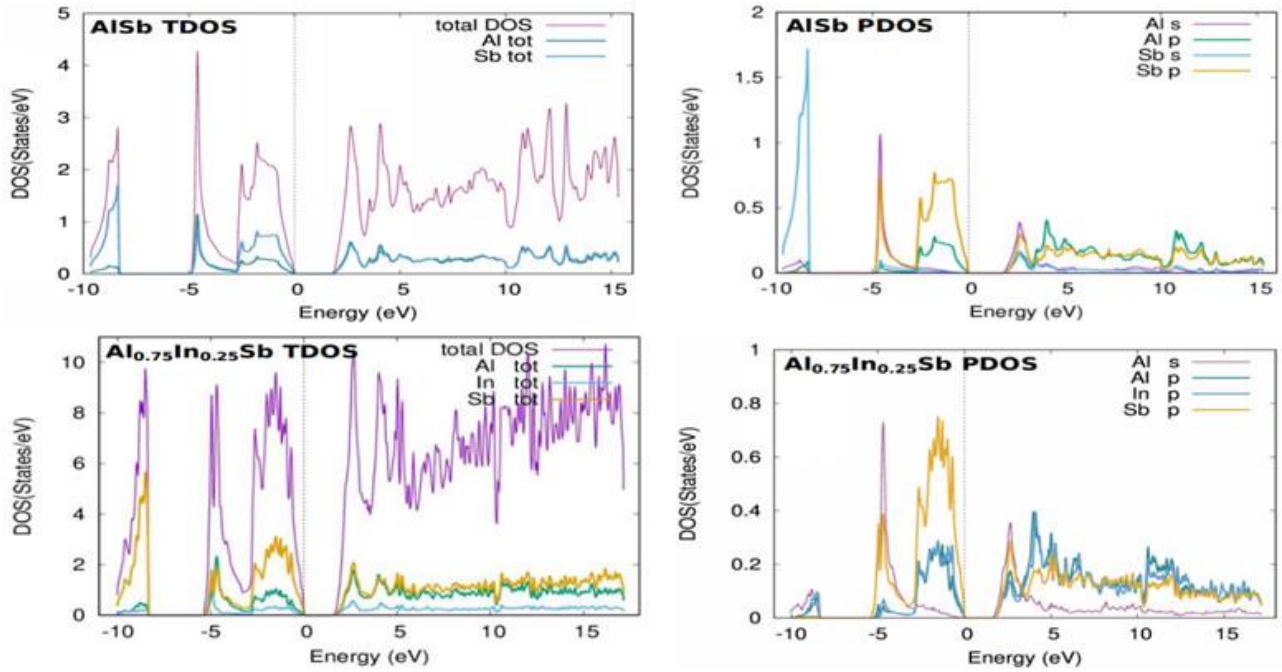


**Figure 7**: Total and partial DOS of binary compound AlSb and ternary alloy $Al_{0.75}In_{0.25}Sb$**.**

The four sections that make up the overall density of the state are the lower valence band (VB) (-10 to -8 eV), the core (-8.1 to -5 eV), the upper valence band (VB) (-5.1 to 0.0 eV), and the conduction band (CB) (1.686 to 15 eV). Indium concentration in pure AlSb increased which lead to a reduction in the band gap between the conduction bands (CB) and the valence band (VB). In figure 7 it is clear that Al-p and Sb-s states in AlSb binary alloy dominate the total density of states in the lower valence band (VB), in contrast to the upper valence band (VB) region Sb-p and Al-s states dominate. In the conduction band (CB) Al-p and Sb-p states constitute a majority of the total density of states for pure AlSb. For $Al_{0.75}In_{0.25}Sb$ lower valance band shows a major contribution of In-s and In-p. In the upper valence band region, the Sb-p and In-s states predominate the overall density of states. But Sb-p and In-p states are more prevailing for the conduction band region.

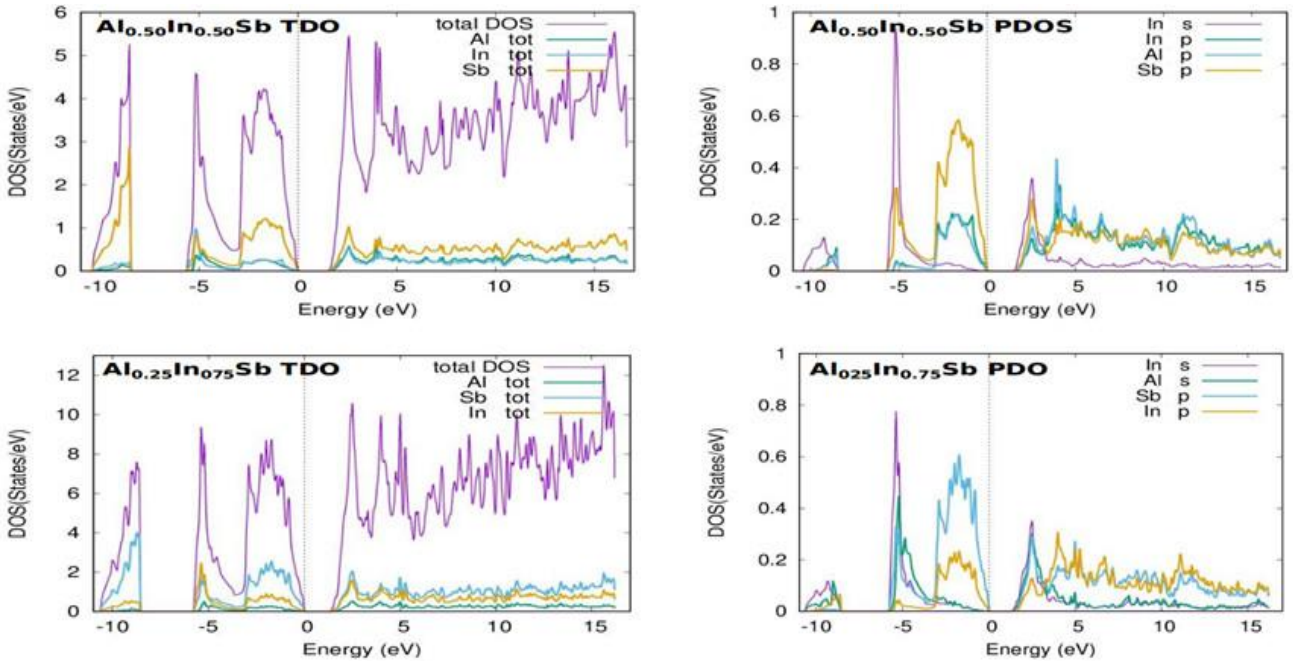


**Figure 8**: Total and partial DOS of ternary alloy $Al_{0.5}In_{0.5}Sb$, $Al_{0.25}In_{0.75}Sb$**.**

$Al_{0.5}In_{0.5}Sb$ and $A1_{0.25}In_{0.75}Sb$ density of states are depicted in Fig. 8. The lower valance band starts at -10 and goes up to 8.5 in $Al_{0.5}In_{0.5}Sb$. There are major contributions of indium-s and aluminum-p-states. The upper valence band extends from $-5.5$ to $0$ eV through which In indicates a significant contribution of p-states and Sb shows a minor donation of s-states of Al. The conduction band (CB) ranges from $0$ to $5$ at $15.5$ with a significant role of Al p, Sb p states, and a small impact of Al-s states. In $Al_{0.25}$ $In_{0.75}Sb$, the range of the lower valence band is between -10.12 and -8.5 eV has major support of In-s state and Sb-p state, with the low role of the Al-p state. The upper valence band extends from $-6.1$ to $0$ eV and displays a larger contribution from In-s and Sb-p and smaller contributions from the In-p and Al-p states. The conduction band (CB) ranges from $1.05$ to $15.5$ eV have a larger role of In-p, Sb-p, and a smaller role of Al-s states.

*3.3. Optical properties*

A material's response to incident light determines its optical characteristics. Semiconductors' optical characteristics are essential for their prospective usage in optoelectronic and photonic applications [33]. The k-points inside the Brillouin zone must be increased for an appropriate computation. So we comprise a Brillion zone of 1000k points[9]. The optical properties of the material are related to its reflectivity, dielectric function, absorption coefficient, optical conductivity, refractive index, and energy loss[42]. The optical properties of ternary alloy $Al_{1-x}In_xSb$ (x = 0.25, 0.50, 0.75) are intended by Claudia Ambrosia-Drawl [9] integrated with the Wien2k package.

*3.3.1 Dielectric function*

The frequency-dependent dielectric function of materials significantly affects the material characteristics. It represents the Fermi sea-like excitation of surface and volume plasmons.

The mathematical relation between real part dielectric function and imaginary part dielectric can be written as [39-40].

$$\varepsilon(\omega) = \epsilon_1(\omega) + i\,\epsilon_2(\omega) \quad (3)$$

*3.3.1.1 Real part of the dielectric function*

The Kramers-Kronig relation is used to define the dielectric function which demonstrates the optical response to all possible photon energies [44].

$$\epsilon_1(\omega) = 1 + \frac{2}{\pi} P \int_0^{\infty} \frac{\omega' \epsilon_2 \omega'^2}{\omega'^2 - \omega^2} d(\omega') \quad (4)$$

At zero frequency the real parts of the dielectric constant for pure AlSb, $Al_{0.75}Ga_{0.25}Sb$, $Al_{0.5}Ga0.5Sb$, and $Al_{0.25}Ga_{0.75}Sb$ are 9.184, 10.322, 10.960, and 12.52 respectively. This quantity reaches its highest point before approaching zero and then shifts toward the negative. For pure AlSb, $Al_{0.75}Ga_{0.25}Sb$, $Al_{0.5}Ga_{0.5}Sb$, and $Al_{0.25}Ga_{0.75}Sb$ the negative energy values are 4.354 eV, 4.35 eV 4.522 eV, and 4.822 eV respectively. At zero energy real component of the dielectric function goes high as the indium atom concentration increases. This demonstrates an inverse relationship between the band gap and dielectric function as determined by the Penn model. [45].

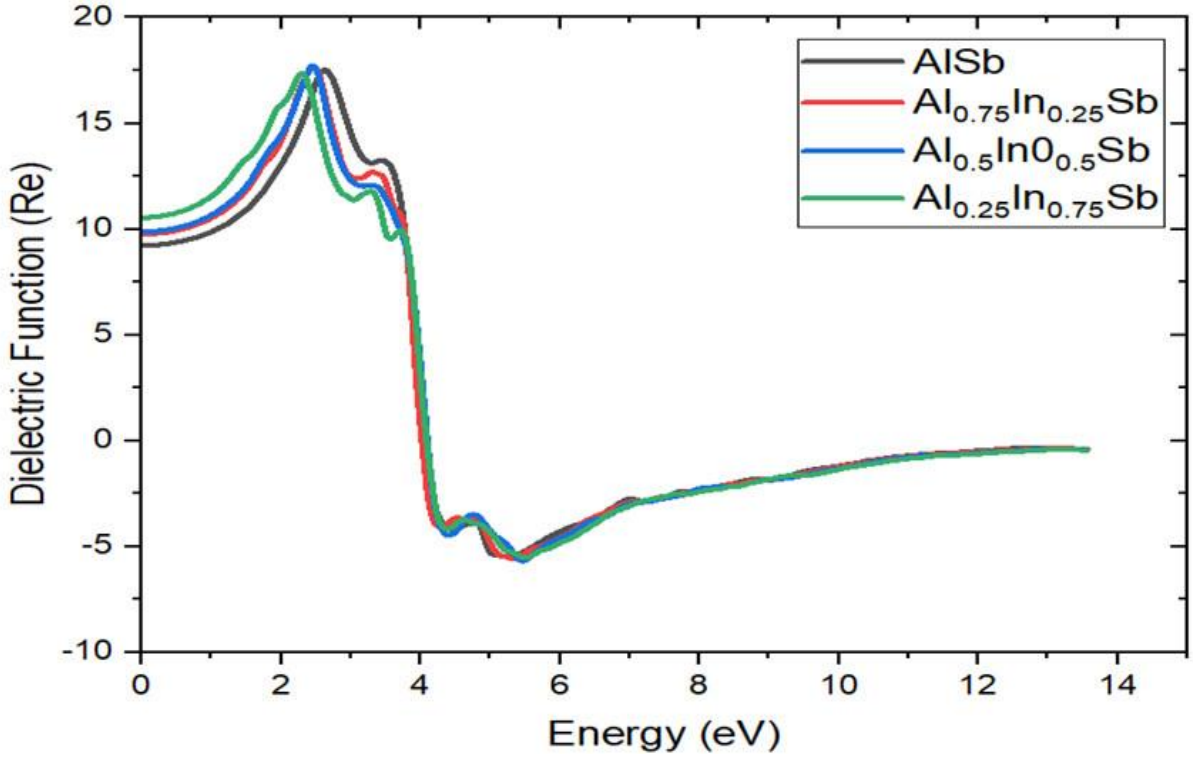


**Figure 9** Real component of dielectric function (energy based) for $AlSb$, $Al_{0.75}\,In_{0.25}\,Sb$, $Al_{0.5}\,In_{0.5}\,Sb$, and $Al_{0.25}\,In_{0.75}\,Sb$.

*3.3.1.2 Imaginary part of dielectric function ε(ω)*

The diectric costant is the efficiency of dielectric material to store the electrical energy and the dielectric loss indicates to loss of electrical enenergy as heat energy.One part represent the energy gain and other represent the energy loss of material in term of electric field. When

electromagnetic radiation is applied to materials the response is renowned complex dielectric function $\boldsymbol{\varepsilon_2}$ that reflects the absorption of the material [2]. The absorption behavior is represented by the imaginary portion of dielectric materials that are closely linked to the electronic band structure of $Al_{1-x}In_xSb$ material[46]. The optical and electronic characteristics of semiconductors are also greatly influenced by complex dielectric functions [40]. The production of optoelectronic components like solar cells and detectors depends heavily on these semiconductor properties [47]. The significant values for the imaginary part of the dielectric function with the value of $x = 0, 0.25, 0.5,$ and $0.75$ are $1.651$ eV, $1.123$ eV $1.074$ eV, and $1.052$ eV. These points are closely associated with the electronic band gap of $1.69$ eV, $1.125$ eV, $1.08$ eV, and $1.05$ eV of $Al_{1-x}In_xSb$. In the dielectric constant, the imaginary part can be measured by using this mathematical equation [46].

$$\epsilon_2(\omega) = \frac{8}{2\pi\omega^2}\sum_{nn}\int \frac{|P_{nn}(k)|^2\ ds_k}{\nabla\omega_{nn}(k)} \tag{5}$$

$\varepsilon_2(\omega)$ is strongly based on the joint density of the $\omega_{nn}$ states and also on the element of the momentum matrix for the first and last state $p_{nn}$ (k), $ds_k$ is the constant value of surface energy. As shown in the figure the imaginary part of the dielectric constant to AlSb and its alloy $Al_{1-x}In_xSb$ (x = 0.25, 0.50, 0.75) is determined over an energy range of 0.0 to 20 eV. The significant peaks for AlSb, $Al_{0.75}Ga_{0.25}Sb$, $Al_{0.5}Ga_{0.5}Sb$, and $Al_{0.25}Ga_{0.75}Sb$ are$32.815$ at $3.862$ eV, $29.399$ at $3.519$ eV, $28.184$ at $3.764$ eV, and $27.434$ at $3.740$ eV, respectively.

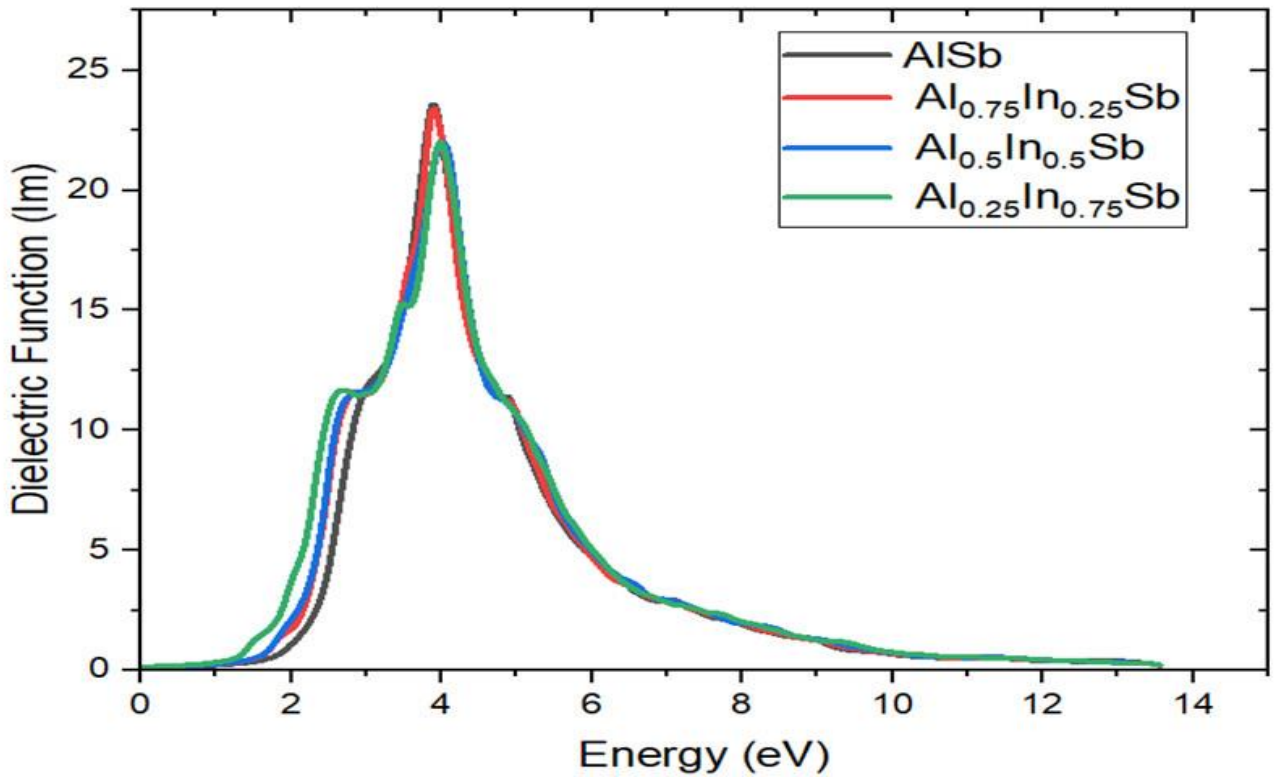


**Figure 10** Imaginary component of dielectric function (energy based) for $AlSb$, $Al_{0.75}\,In_{0.25}\,Sb$, $Al_{0.5}\,In_{0.5}\,Sb$, and $Al_{0.25}\,In_{0.75}\,Sb$.

*3.3.2 Refractive index*

The quantity of light that is refracted by a substance is determined by its refractive index, which is strongly tied to infinitesimal atomic interactions[48]. A key factor known as the material's refractive index plays a vital role in the design of industrial optical materials including optical thin films, optical lenses, and pigments. The refractive index of the material is the measure of its transparency to the incident photon [3]. The dielectric function's real and imaginary parts are used to compute the refractive index.[45].

$$n(\omega) = n(\omega) + ik(\omega) = \sqrt{\varepsilon(\omega)} = \sqrt{\varepsilon_1(\omega) + i\varepsilon_2(\omega)} \quad (6)$$

The terms "index of refraction (frequency dependent) $n(\omega)$" and "extinction coefficient (frequency dependent) $k(\omega)$ " refer to the optical constants n and k, respectively [46]. The real portion of a refracted index (frequency dependent) $n(\omega)$ and the imaginary part extinction coefficient $k(\omega)$ are deliberated as

$$n(\omega) = \frac{1}{\sqrt{2}} \sqrt{\{\varepsilon_1\omega^2 + \varepsilon_2\omega^2\}^{1/2} + \varepsilon_1(\omega)} \quad (7)$$

$$k(\omega) = \frac{1}{\sqrt{2}} \sqrt{\{\varepsilon_1\omega^2 + \varepsilon_2\omega^2\}^{1/2} - \varepsilon_1(\omega)} \quad (8)$$

The calculated refractive indices of $Al_{1-x}In_xSb$ are illustrated in the figure

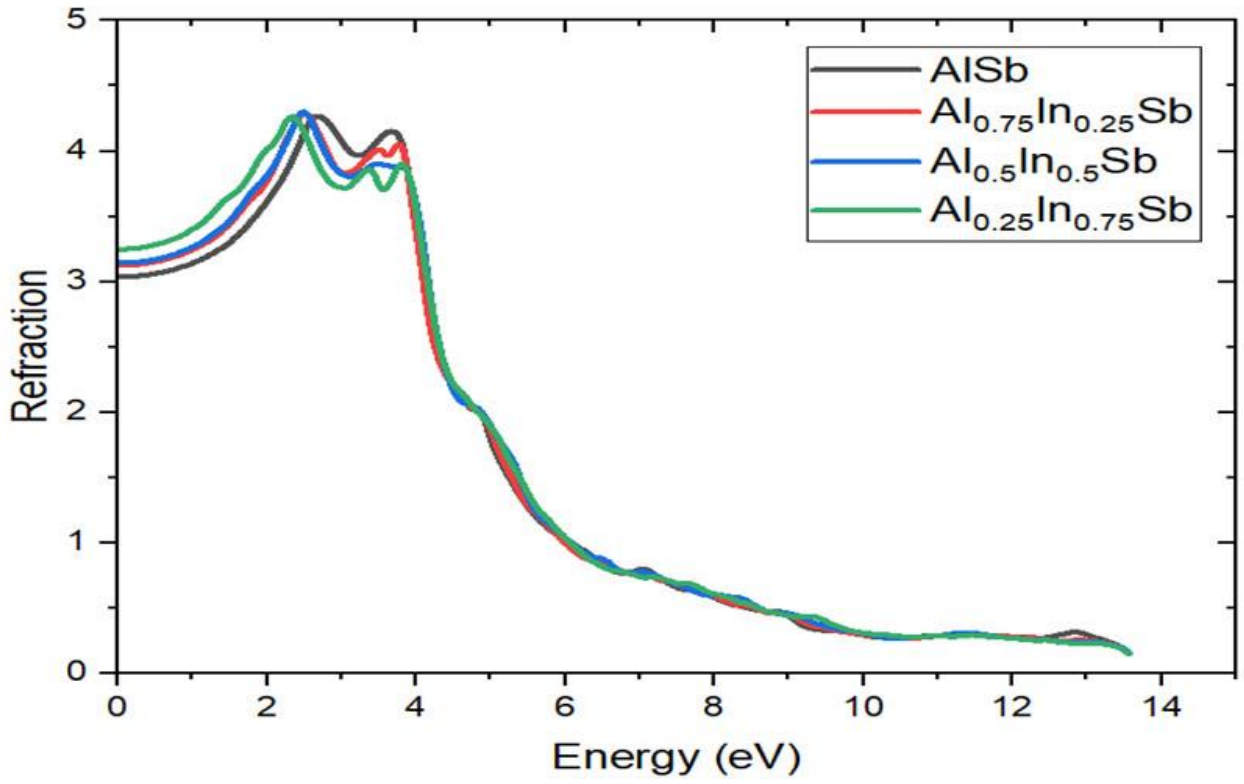


**Figure 11** Energy-based refraction of AlSb, $Al_{0.75}In_{0.25}Sb$, $Al_{0.5}In_{0.5}Sb$, and $Al_{0.25}In_{0.75}Sb$**.**

The spectrum of refractive indices roughly resembles the real portion of the dielectric constant. Figure 11 shows that when the indium concentration in $Al_{1-x}$ $In_xSb$ (x = 0.25, 0.50, 0.75) grows, the refractive index rises as well. At zero frequency band gap of $Al_{1-x}In_xSb$ is inversely related to the refractive. The zero frequency limits of refractive indices for pure AlSb, $Al_{0.75}Ga_{0.25}Sb$, $Al_{0.5}Ga_{0.5}Sb$, and $Al_{0.25}Ga_{0.75}Sb$ are 3.033, 3.217, 3.296, and 3.515

respectively. The greatest value of the refractive index (n) is between 2.686 and 4.250 eV for pure binary alloy AlSb, between 2.269 and 4.18 eV for $Al_{0.75}In_{0.25}Sb$, between 2.147 and 4.259 eV for $Al_{0.5}In_{0.5}Sb$ and between 1.950 and 4.382 eV for $Al_{0.25}In_{0.75}Sb$. The maximum value of refractive indices decreases and falls to below 1. The reason for this decrease in higher energy value is that material is no longer transparent and absorbs high-energy photons. If the refractive index is below value Vg = c / n then the group velocity of the incoming electromagnetic radiation into the material is greater than C. This indicates that the material's nature shifts from linear to nonlinear and the group velocity enters the negative range. In a nutshell, matter turns into superluminal for high-energy photons.

*3.3.3 Reflectivity*

Reflectivity is regarded as a vital optical property that elaborates how material' surfaces respond to electromagnetic waves plays a dynamic role in the characterization of a material and it possible applications[49]. The ratio of the power of light reflected the power of light incident on the surface of a material is known as reflectivity. The relationship is used to compute the reflectance using n(ew) and k(w) known as optical parameters [50].

$$R(\omega) = \left|\frac{n(\omega)-1}{n(\omega)+1}\right| = \frac{(n(\omega)-1)^2 + k(\omega)^2}{(n(\omega)+1)^2 + k(\omega)^2} \quad (9)$$

where $k(\omega)$ represents the extinction coefficient and $n(\omega)$ represents the real component of the refractive index [50]. Fig. 13 shows the calculated reflectance as a function of energy.

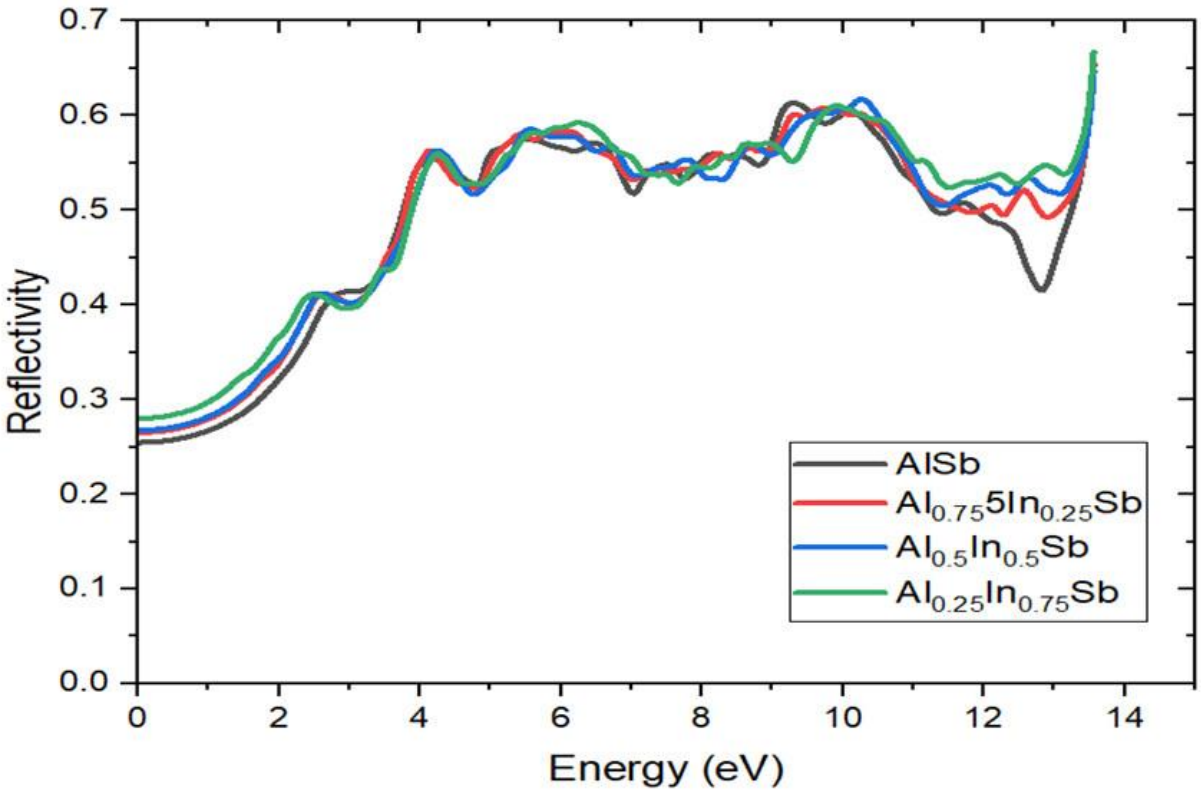


**Figure 12** Energy based reflectivity of of $AlSb$, $Al_{0.75}\,In_{0.25}\,Sb$, $Al_{0.5}\,In_{0.5}\,Sb$ and $Al_{0.25}\,In_{0.75}\,Sb$.

The figure shows the maximum reflectance value at different frequencies. The Maximum values of energy lie between 0.0 to 20 eV. The zero-frequency limit of reflection for $Al_{1-x}In_xSb$ *(x = 0.25, 0.50, 0.75)* changes with Indium concentration. The reflectance at zero frequency limits for pure AISb, $Al_{0.75}In_{0.25}Sb$, $Al_{0.5}In_{0.5}Sb$, and $Al_{0.25}In_{0.75}Sb$ are 0.253, 0.274, 0.2866, and 0.310, correspondingly.

*3.3.4 Optical conductivity*

When the light of appropriate frequency hits on the surface of a material, electronic conduction starts corresponding property of the material is said to be optical conductivity denoted by σ (ω). The optical conductivity spectrum σ(ω) is derived from the complex dielectric function $\varepsilon_2(\omega)$. Optical conductivity provides a base for the prediction and application of semiconductor material [7].The optical conductivity is reciprocal to optical resistivity also as optical conductivity increases than optical resistivity decreases and vice versa. The optical conductivity is calculated using the equation [51]. The deliberated optical conductivity (Mainly dependent upon frequency) for $Al_{1-x}In_xSb$ (x = 0.25, 0.50, 0.75) is illustrated in Fig. 14

$$\sigma_{\omega} = 2\omega_{ev}\frac{\hbar}{E_0} \quad (10)$$

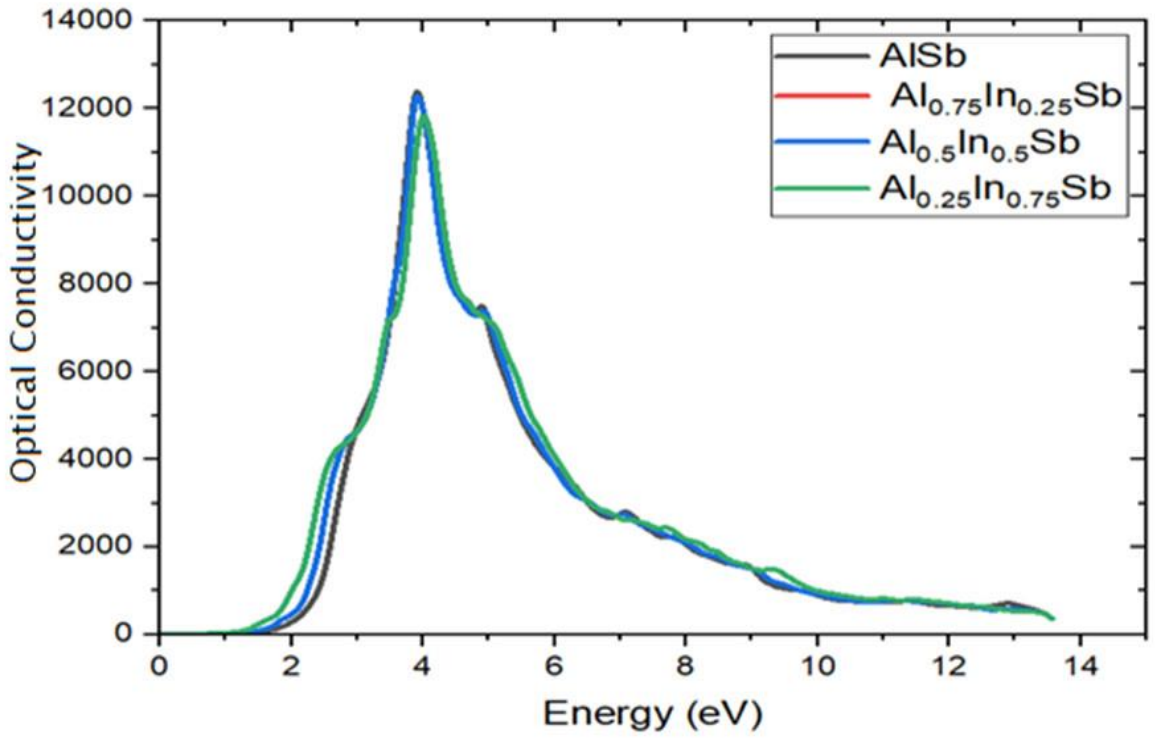


**Figure 13** Energy based optical conductivity of AlSb, $Al_{0.75}$ $In_{0.25}$ Sb, $Al_{0.5}$ $In_{0.5}$ Sb and $Al_{0.25}$ $In_{0.75}$ Sb.

It can be seen from Figure 13 that the analog peak of optical conductivity shifts to higher energies as the Indium concentration increases. Maximum values $12310.9\ 015\ \Omega^{-1}\ m^{-1}$ at 3.936 eV for AlSb, $1052.2\ 015\ \Omega^{-1}\ m^{-1}$ at 4.034 eV for $Al_{0.75}$ $In_{0.25}$ Sb, $9516.8\ 015\ \Omega^{-1}\ m^{-1}$ at 4.132 eV for $Al_{0.5}$ $In_{0.5}$ Sb and $10280015\ \Omega^{-1}\ m^{-1}$ at 3.740 eV for $Al_{0.25}$ $In_{0.75}$ Sb.

*3.3.5 Absorption Coefficient*

When the photon energy of the incoming beam exceeds the band gap the electromagnetic waves are absorbed. In absorption, there is a loss of radiant energy by radiations but gained by the molecules or atoms of material [24]. When the radiations are get absorbed then the vibrational energy of particles increases within the material. The absorption coefficient can be calculated from this dielectric function.

$$\alpha(\omega) = \quad 2\omega k(\omega) = \sqrt{2\omega}\ \sqrt{\{\varepsilon_1\omega^2 + \ \varepsilon_2\omega^2\}^{1/2} - \varepsilon_1(\omega)} \tag{11}$$

The absorption coefficient can be calculated by using Beer's Law having a mathematical expression as [52].

$$\alpha(\omega) = \frac{2\omega k}{c} \tag{12}$$

Absorption coefficient (mainly depending upon frequency) for $Al_{1-x}Ga_xSb$ (x = 0.25, 0.50, 0.75) is illustrated in Fig. 14.

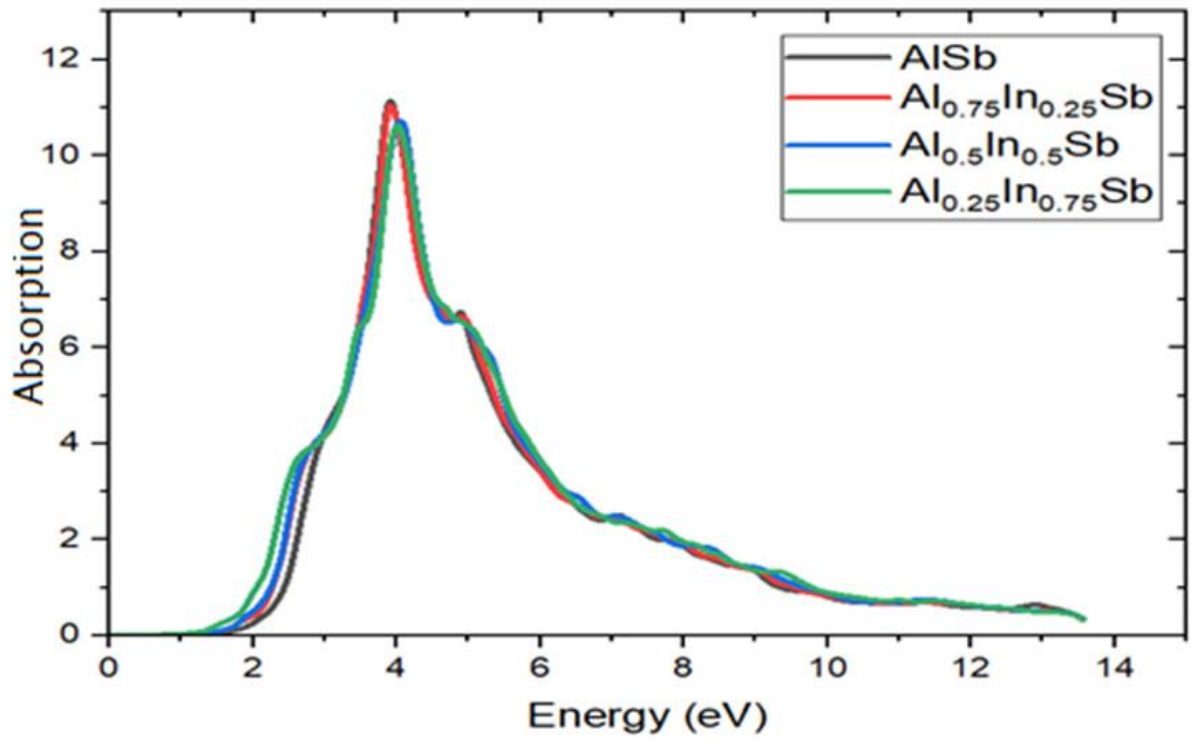


**Figure 14** Energy based Absorption of $AlSb$, $Al_{0.75}\,In_{0.25}\,Sb$, $Al_{0.5}\,In_{0.5}\,Sb$ and $Al_{0.25}\,In_{0.75}\,Sb$.

The highest peak having the value of absorption is $11.015\ \mathrm{Cm^{-1}}$ at $3.936$ eV for AlSb, $9.376\ \mathrm{Cm^{-1}}$ at $4.304$ eV for $Al_{0.75}\,In_{0.25}\,Sb$, $8.549\ \mathrm{Cm^{-1}}$ at $4.032$ eV for $Al_{0.5}\,In_{0.5}\,Sb$ and $9.217\ \mathrm{Cm^{-1}}$ at $3.740$ eV for $Al_{0.25}\,In_{0.75}\,Sb$.

*3.3.6 Transmittance*

Optical transmittance represents the transmission of electromagnetic waves through material. Fig. 15 depicts the optical transmittance curves for AlSb, $Al_{0.75}\,In_{0.25}\,Sb$, $Al_{0.5}\,In_{0.5}\,Sb$ and $Al_{0.25}\,In_{0.75}\,Sb$. The material's maximum transperancy is demonstrated by the optical transmittance is 145 at 5.5 eV. Transmittance falls as electromagnetic wave frequency increases. In a limited number of optical applications, this property can be used[53].

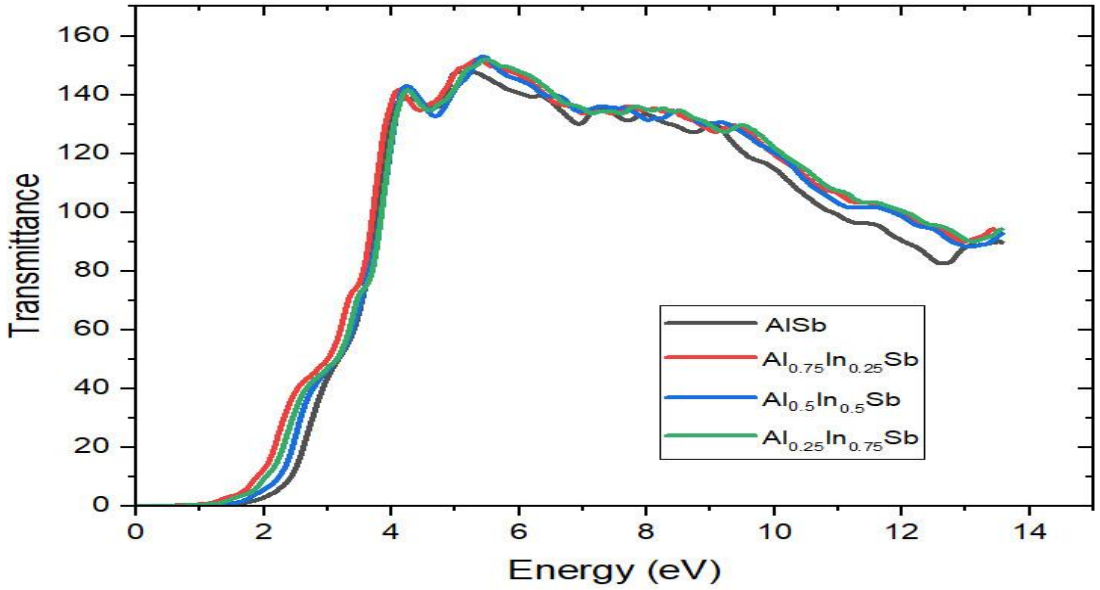


**Figure 15** Energy based Transmittance of $AlSb$, $Al_{0.75}\,In_{0.25}\,Sb$, $Al_{0.5}\,In_{0.5}\,Sb$ and $Al_{0.25}\,In_{0.75}\,Sb$.

*3.3.7 Loss of energy*

The energy loss function defines the energy loss which is used to determine the plasmon energy. The dielectric function can be used to calculate the energy lost as the radiation travels through the medium[2].

$$L(\omega) = -lm\left(\frac{1}{\varepsilon(\omega)}\right) = \frac{\varepsilon_{2}\ (\omega)}{\varepsilon_1\omega^2 + \varepsilon_2\omega^2} \quad (13)$$

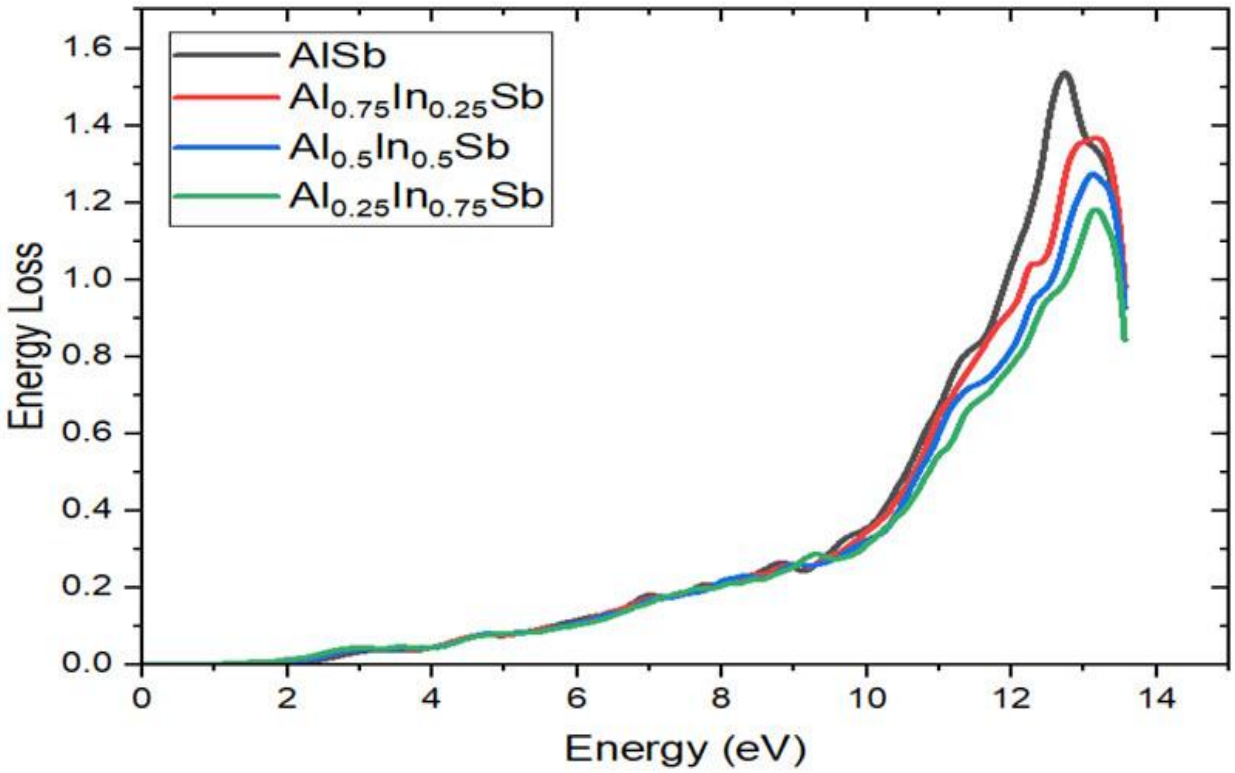


**Figure 16** Energy-based optical energy loss of AISb, $Al_{0.75}In_{0.25}Sb$, $Al_{0.5}In_{0.5}Sb$, and $Al_{0.25}In_{0.75}Sb$.

A strong peak is observed for the energy loss function that shows as a concentration of Indium increases, the peak decreases and shifts to a lower energy limit. The energy loss for $Al_{1-x}In_xSb$ *(x = 0.25, 0.50, 0.75)* is at most in the range of 10 to 15 eV. The pure binary alloy AlSb has the highest value range of energy loss at 1.528 at 12.5 eV, similarly, the ternary alloy $Al_{0.75}Ga_{0.25}Sb$ has an energy loss of 1.427 at 12.6 eV, 1.409 at 12.7 eV for $Al_{0.5}Ga_{0.5}Sb$, and 1.409 at 12.7 eV for $Al_{0.25}Ga_{0.75}Sb$.

## 4. CONCLUSIONS

The structural properties, electronic properties, and optical properties of pure Binary alloy AlSb and its ternary (Doped) alloy $Al_{1-x}In_xSb$ are examined using density functional with the assistance of Wien2K. Structural properties are based upon parameters like pressure derivative, bulk modulus, and lattice constant are calculated using the Murnaghan equation of state. The computed structural property results show that the lattice constant and bulk modulus in pure AlSb increases as the indium concentration increases. GGA-PBE uses the TB-mBJ technique to calculate electronic parameters including band structure and density of states. Electronic properties analysis demonstrates that AlSb exhibits an indirect band-gap (r-L) and is an optically inactive material. The band gap decreases and switches from indirect to direct when we increase indium concentration (0.25, 0.5, and 0.75) which makes the material optically active (r-r). Band-gap shows direct relation to the imaginary part of the dielectric function but shows inverse relation to the real dielectric function. Reflectivity and index of refraction show the indirect relationship to band-gap. At zero frequency reflectivity and refractive index increase as the Indium concentration in pure AlSb increases. Optical conductivity and absorption show direct relation with band-gap. At zero o frequency optical conductivity and absorption decrease as indium concentration increases. The energy loss also

gets minimal by growing the indium concentration in pure AlSb. Evaluation of structural electronic and optical properties such as band gap reduction, indirect to direct bandgap conversion, increased refractive index (n) and reduced energy loss by increasing Indium ratio in pure AlSb shows that $Al_{1-x}In_xSb$ ternary alloy is of paramount significance and should be extremely beneficial for optoelectronic devices and photonic uses i.e. for the manufacturing of p-n junctions, photo-detectors, laser, photo-diodes, transistors and solar spectrum absorptions in the visible, infrared and ultraviolet energy ranges.

**References**

[1] X. Wang, W. Liu, C. Zhai, J. Yun, Z. Zhang, Medziagotyra 26 (2020) 127
[2] S. Touam et al., Bull. Mater. Sci. 43 (2020) 1
[3] M. Zafar et al., Optik 182 (2018) 1176
[4] A. Bentayeb et al., J. Comput. Electron. 18 (2019) 791
[5] B. Owens-Baird et al., J. Am. Chem. Soc. 142 (2020) 2031
[6] M. A. ALI, N. Khan, F. Ahmad, A. Ali, M. Ayaz, Bull. Mater. Sci. 42 (2019) 1
[7] Z. Zhang, C. Chai, Y. Song, L. Kong, Y. Yang, Mater. Res. Express 8 (2021) 25908
[8] M. A. Ali, H. Aleem, B. Sarwar, G. Murtaza, Indian J. Phys. 94 (2020) 477
[9] M. C. Benesten, C. J. Thordor, C. Anderson, Exp. Theo. NANOTECHNOLOGY 4 (2020) 67
[10] A. Hanson, A. Motengen, Exp. Theo. NANOTECHNOLOGY 4 (2020) 75
[11] K. Turjak, D. Lapčík, Exp. Theo. NANOTECHNOLOGY 4 (2020) 81
[12] Y. Mao, X. X. Liang, G. J. Zhao, T. L. Song, Phys. B Phys. Condens. Matter 569 (2019) 87
[13] D. M. Hoat, J. F. Rivas Silva, A. Méndez Blas, Solid State Phys. 382 (2018) 1942
[14] L. Needs, K. Willams, Exp. Theo. NANOTECHNOLOGY 4 (2020) 93
[15] G. Rehman et al., J. Electron. Mater. 45 (2016) 3314
[16] C. G. Ma and M. G. Brik, Comput. Mater. Sci. 58 (2012) 101
[17] R. Ahmed, Fazal-e-Aleem, S. J. Hashemifar, and H. Akbarzadeh, Phys. B Condens. Matter 403 (2008) 1876
[18] Z. Ali, I. Khan, M. Rahman, R. Ahmad, I. Ahmad, Opt. Mater. 58 (2016) 466
[19] A. M. Ahmed Alwaise, M. Ibrahim Alwiase, A.Y.Qasim, Exp. Theo. NANOTECHNOLOGY 4 (2020) 99
[20] H. Bennacer, A. Boukortt, S. Meskine, M. Hadjab, M. I. Ziane, A. Zaoui, Optik 159 (2018) 229
[21] F. Annane et al., Pramana - J. Phys. 94 (2020) 1
[22] A. Kafi, F. D. Khodja, F. Saadaoui, S. Chibani, A. Bentayeb, M. D. Khodja, Mater. Sci. Semicond. Process. 113 (2020) 105049
[23] G. Rahman, S. Cho, and S. C. Hong, Phys. Status Solidi Basic Res. 244 (2007) 4435
[24] S. Berrah, A. Boukortt, and H. Abid, Phys. E Low-Dimensional Syst. Nanostructures 41 (2009) 701
[25] A. Hassani, S.A. Hussain, N. Abdullah, S. Kmaruddin, M.K. Alomar, A. Rasedee, M. Al-Qubaisi, R. Rosli, Exp. Theo. NANOTECHNOLOGY 4 (2020) 109
[26] R. Ahmed, S. Javad Hashemifar, H. Akbarzadeh, M. Ahmed, Fazal-e-Aleem, Comput. Mater. Sci. 39 (2007) 580
[27] D. Koller, F. Tran, P. Blaha, Phys. Rev. B 83 (2011) 195134
[28] I. Hattabi, A. Abdiche, F. Semari, R. Khenata, F. Soyalp, Chinese J. Phys. 56 (2018) 2332
[29] B. Bencherif et al., Mol. Phys. 82 (2019) 1
[30] I. Vurgaftman, J. R. Meyer, L. R. Ram-Mohan, J. Appl. Phys. 89 (2001) 5815